JOURNAL OF GUIDANCE, CONTROL, AND DYNAMICS
Vol. 32, No. 4, July–August 2009

Nonlinear Optimization of Low-Thrust Trajectory for Satellite Formation: Legendre Pseudospectral Approach

Baolin Wu* and Danwei Wang†
Nanyang Technological University, Singapore 639798, Republic of Singapore
Eng Kee Poh‡
Defence Science Organization National Laboratories, Singapore 118230, Republic of Singapore
and
Guangyan Xu§
Nanyang Technological University, Singapore 639798, Republic of Singapore

DOI: 10.2514/1.37675

In this paper, we focus on the design of a fuel-optimal maneuver strategy to reconfigure satellite formation using a low-thrust propulsion system. We cast it as an optimization problem with a desired final satellite formation configuration subject to collision avoidance constraints on the paths of the chief and all deputy satellites. The satellite terminal orbit states corresponding to this desired formation configuration are ensured by imposing an energy-matching condition and final geometry configuration constraints in the problem formulation. In addition, we adopt our recently developed relative satellite kinematics model to accurately describe relative satellite orbit geometry in the presence of J_2 effects. The resulting nonlinear optimal control problem is converted into a nonlinear programming problem by the application of the Legendre pseudospectral method and is then solved by using a sparse nonlinear optimization software named TOMLAB/SNOPT. Simulation results demonstrate the efficiency of our proposed method in designing fuel-optimal maneuvers for a wide class of satellite formation problems.

Nomenclature

a_x	=	control acceleration in the x direction
a_y	=	control acceleration in the y direction
a_z	=	control acceleration in the z direction
d	=	distance between satellites
$d_{\max}$	=	possible maximum relative distance during the maneuver
d_{safe}	=	assumed safe distance between satellites
g_0	=	sea level acceleration due to gravity
$\boldsymbol{h}$	=	angular momentum vector of chief satellite
h	=	magnitude of angular momentum vector
I_{sp}	=	specific impulse of the engine
i	=	inclination
J_2	=	geopotential coefficient representing Earth's oblateness
m	=	spacecraft mass
N	=	number of Legendre–Gauss–Lobatto points
N_s	=	number of deputy satellites
R	=	radius of circular formation
$\boldsymbol{r}$	=	position vector of chief satellite
r	=	geocentric distance of chief satellite
T	=	magnitude of constant thrust
T_c	=	period of chief satellite
u	=	thrust direction
x	=	radial difference between two objects in the local-vertical–local-horizontal frame
y	=	along-track difference between two objects in the local-vertical–local-horizontal frame
z	=	cross-track difference between two objects in the local-vertical–local-horizontal frame
θ	=	true latitude

Subscripts

f	=	final value
j	=	the jth deputy satellite
0	=	initial value

Superscripts

υ	=	the υth phase in the trajectory
$\sim$	=	scaled variable

Presented at the AAS/AIAA 18th Space Flight Mechanics Meeting, Galveston, Texas, 27–31 January 2008; received 23 March 2008; revision received 14 January 2009; accepted for publication 6 March 2009.

*Ph.D. Student, Aerospace Electronics Laboratory School of Electrical and Electronics Engineering; wuba0001@ntu.edu.sg.
†Professor, School of Electrical and Electronics Engineering; edwwang@ntu.edu.sg.
‡Distinguished Member of Technical Staff.
§Research Fellow, School of Electrical and Electronics Engineering.

I. Introduction

SATELLITE formation flying consists of multiple satellites for which the dynamics are coupled through a common control law [1]. Because of its perceived operational benefits (e.g., decreased cost, mission flexibility, improved performance, increased reliability, and enhanced survivability) as compared with a single, conventional, large satellite, formation flying has been identified as a key enabling technology for many defense- and science-based missions. However, there are several technical challenges that such missions face: high-precision relative navigation, distributed communication, fault detection, path planning, and control. Specifically, the planning and control problems can be decomposed into two tasks: 1) formation keeping to maintain the satellites in stable formation to within specified precision against various orbital perturbations, and 2) formation maneuver to reconfigure from existing satellite formation to another stable formation. The trajectory optimization problem for formation maneuver is addressed in this paper.

Trajectory optimization is critical to stable initial satellite formation deployment and successful subsequent formation reconfiguration. Based on the type of the thruster used, trajectory optimization techniques for satellite formation can be roughly categorized into two main approaches: 1) impulsive control, which relies on chemical thrusters; and 2) continuous low-thrust control, which uses electric

propulsion systems. Impulsive control methods for formation establishment and reconfiguration are proposed in [2–4]. Continuous low-thrust control methods are now actively investigated for satellite formation control. The main advantages are that low-thrust engines (such as the ion thruster and the plasma thruster) can generate precise thrust output and consume less propellant due to their high specific impulse. Recent advances in the field of electric propulsion have made low-thrust propulsion an operational reality [5,6].

Tillerson et al. [7] proposed a fuel/time-optimal solution for formation reconfiguration by solving a linear programming problem. To guarantee safe maneuvering among satellites, Richards et al. [8] extended the aforementioned method to include collision avoidance by using a mixed-integer linear programming approach. The necessary logical constraints for collision avoidance are appended to a fuel-optimizing linear programming problem by including binary variables in the optimization. Açıkmeşe et al. [9] presented a convex guidance algorithm for optimal formation reconfiguration with collision avoidance based on heuristic reasoning. Campbell [10] proposed a methodology using Hamilton–Jacobian–Bellman optimality to generate a set of fuel- or time-optimal trajectories from an initial stable formation to a final stable formation in circular orbits. The result was subsequently extended to satellite formations in elliptic orbits [11].

Linear relative dynamics models were used in all the works mentioned. However, linearized relative motion equations ignore significant orbital perturbations due to the Earth's oblateness, that is, the J_2 effect. To obtain high-precision formation maneuver trajectories, some researchers investigated nonlinear trajectory optimization with a nonlinear satellite orbit dynamic model. Milam et al. [12] used the nonlinear trajectory generation (NTG) software package to generate constrained trajectories for satellite formation keeping and reconfiguration. A sequential quadratic programming software, NPSOL, was used to solve the nonlinear programming problem in NTG. Huntington et al. [13] and Huntington and Rao [14] proposed a nonlinear fuel-optimal configuration and reconfiguration method for tetrahedral formation using the Gauss pseudospectral method (GPM), but collision avoidance was not addressed. The satellite orbit dynamics models used in these two methods use a Gauss variational equation to describe each satellite orbit rather than their relative orbit dynamics. This introduces a severe computational challenge, because numerical calculations must be done with a high degree of accuracy. Furthermore, it is difficult to include collision avoidance and formation configuration constraints by using an absolute satellite orbit dynamics model. Mauro and Franco [15] proposed an optimal nonlinear low-thrust trajectory for formation flying using a parallel multiple shooting method. The problem was transcribed into a nonlinear programming problem and solved with an interior point algorithm. However, the final relative state for each satellite was restricted to only permissible a priori fixed states.

This paper aims to develop fuel-optimal low-thrust trajectories for high-precision formation maneuver using an exact nonlinear relative satellite dynamics model with orbital eccentricity and Earth oblateness effects. To maneuver the satellites to a bounded desired formation, an energy-matching condition and final geometry configuration constraints are included in the optimization formulation. Furthermore, collision avoidance constraints are introduced to guarantee the safe maneuvering of satellites. The problem is then numerically solved by a direct transcription technique called the Legendre pseudospectral method (LPM) [16].

Numerical methods for solving the trajectory optimization problem can be grouped into two major categories: indirect methods and direct methods. A comprehensive survey of various numerical methods for solving trajectory optimization problems can be found in [17]. In indirect methods, the optimality conditions are derived using a calculus of variations. These necessary conditions lead to a nonlinear multipoint boundary-value problem. The main drawbacks of the indirect method are that the radius of convergence is usually very small and it is difficult to analytically derive the optimality condition for a complex problem [17]. In direct methods, the nonlinear system dynamics model is discretized into a set of algebraic constraints and the trajectory optimization problem is converted into a nonlinear programming problem (NLP). An NLP can be solved using an appropriate optimization method, such as those described in [17]. Common discretization methods used in direct methods include trapezoidal, Hermite–Simpson, and Runge–Kutta methods. Direct methods are actively investigated by many researchers. There are two main reasons for the widespread use of direct methods. First, they can be applied without explicitly deriving the necessary optimality conditions. Second, direct methods do not require a prior specification of the arc sequence for problems with path inequalities.

In particular, a direct method that has shown tremendous promise is the LPM [16,18]. It has been applied to a wide variety of applications including atmospheric entry [19], orbital transfer [20], spacecraft formation design [21], trajectory design for a launch vehicle [22], and satellite attitude control [23]. In the LPM, the continuous state and control variables are approximated using a basis of globally orthogonal polynomials, which results in improved accuracy and a faster speed of convergence. The pseudospectral differentiation matrix then provides a numerical estimation of the derivatives at the Legendre–Gauss–Lobatto (LGL) points. Thus, for our present problem, the differential equations of relative satellite motion can be converted into a nonlinear programming problem.

This paper is organized as follows. First, the exact nonlinear relative dynamics for satellite formation maneuver is introduced. Second, the formulation of the trajectory optimization problem for satellite formation is presented. Third, the LPM is briefly reviewed. Thereafter, computational implementation issues are discussed. Finally, comprehensive simulation results are presented for the validation of the proposed trajectory optimization method using MATLAB® and TOMLAB/SNOPT [24].

II. Equation of Relative Motion

To generate high-precision formation maneuver trajectories, a high-fidelity relative dynamics model is required. An exact nonlinear relative dynamics model developed by Xu and Wang [25] is used in this paper. In the presence of only J_2 perturbation, these developed dynamic equations are exact in describing the relative satellite motion in any eccentric orbits. Although it is beyond the scope of this paper to provide a detailed explanation of the exact relative dynamics, a brief description is given here. The reader is referred to [25] for further details of the dynamics model.

Firstly, a local-vertical–local-horizontal (LVLH) frame, shown in Fig. 1, is defined with its origin located at the position of the chief satellite and with the coordinate system spanned by the unit vectors

$$\hat{\mathbf{x}} = \mathbf{r}/r \qquad \hat{\mathbf{z}} = \mathbf{h}/h \qquad \hat{\mathbf{y}} = \hat{\mathbf{z}} \times \hat{\mathbf{x}} \tag{1}$$

The J_2 nonlinear ordinary differential equations describing relative satellite motion are as follows:

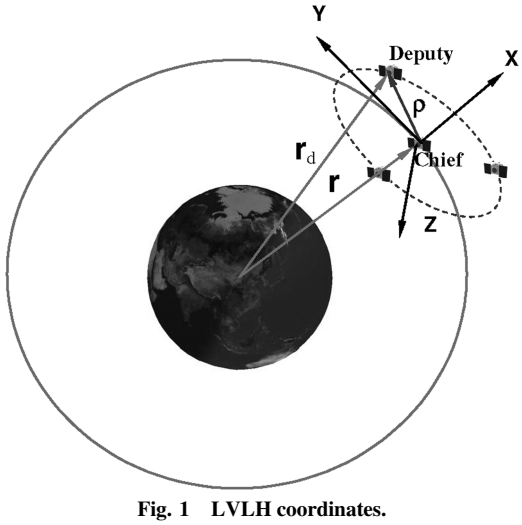

Fig. 1 LVLH coordinates.

$$\ddot{x}_j = 2\dot{y}_j\omega_z - x_j(\eta_j^2 - \omega_z^2) + y_j\alpha_z - z_j\omega_x\omega_z - (\zeta_j - \zeta)\sin i\sin\theta - r(\eta_j^2 - \eta^2) + a_{j,x}$$
$$\ddot{y}_j = -2\dot{x}_j\omega_z + 2\dot{z}_j\omega_x - x_j\alpha_z - y_j(\eta_j^2 - \omega_z^2 - \omega_x^2) + z_j\alpha_x - (\zeta_j - \zeta)\sin i\cos\theta + a_{j,y}$$
$$\ddot{z}_j = -2\dot{y}_j\omega_x - x_j\omega_x\omega_z - y_j\alpha_x - z_j(\eta_j^2 - \omega_x^2) - (\zeta_j - \zeta)\cos i + a_{j,z} \tag{2}$$

where (ω_x, ω_z) and (α_x, α_z) are the angular velocities and accelerations of the chief satellite given by

$$\omega_x = -k_{J2}(\sin 2i\sin\theta)/(hr^3) \tag{3}$$

$$\omega_z = h/r^2 \tag{4}$$

$$\alpha_x = -k_{J2}(\sin 2i\cos\theta)/r^5 + 3v_x k_{J2}(\sin 2i\sin\theta)/(r^4 h) - 8k_{J2}^2\sin^3 i\cos i\sin^2\theta\cos\theta/(r^6h^2) \tag{5}$$

$$\alpha_z = -2hv_x/r^3 - k_{J2}(\sin^2 i\sin 2\theta)/r^5 \tag{6}$$

with n^2, n_j^2, ζ_j, and ζ defined as follows:

$$n^2 = \mu/r^3 + k_{J2}/r^5 - 5k_{J2}\sin^2 i\sin^2\theta/r^5 \tag{7}$$

$$n_j^2 = \mu/r_j^3 + k_{J2}/r_j^5 - 5k_{J2}r_{jZ}^2/r_j^7 \tag{8}$$

$$\zeta_j = 2k_{J2}r_{jZ}/r_j^5, \qquad \zeta = 2k_{J2}(\sin i\sin\theta)/r^4 \tag{9}$$

In these equations, r, v_x, h, i, and θ are solutions to the following dynamic equations:

$$\dot{r} = v_x$$
$$\dot{v}_x = -\mu/r^2 + h^2/r^3 - k_{J2}(1 - 3\sin^2 i\sin^2\theta)/r^4$$
$$\dot{h} = -k_{J2}(\sin^2 i\sin 2\theta)/r^3$$
$$\dot{\theta} = h/r^2 + 2k_{J2}(\cos^2 i\sin^2\theta)/(hr^3)$$
$$\dot{i} = -k_{J2}(\sin 2i\sin 2\theta)/(2hr^3) \tag{10}$$

with

$$k_{J2} = 3J_2\mu R_e^2/2 \tag{11}$$

$$r_j = \sqrt{(r + x_j)^2 + y_j^2 + z_j^2} \tag{12}$$

$$r_{jZ} = (r + x_j)\sin i\sin\theta + y_j\sin i\cos\theta + z_j\cos i \tag{13}$$

For the application under consideration here, the control accelerations are written as

$$a_{j,x} = T_j u_{j,x}/m_j, \qquad a_{j,y} = T_j u_{j,y}/m_j, \qquad a_{j,z} = T_j u_{j,z}/m_j \tag{14}$$

During the burn phase of maneuver trajectory, the thrust magnitude is constant, but the thrust direction is steerable. Finally, the mass flow rate of the engine is described by the following equation:

$$\dot{m}_j(t) = -T_j/(g_0 I_{sp}) \tag{15}$$

III. Problem Formulation

The trajectory optimization problem for a fuel-optimal satellite formation maneuver can be formulated as follows.

Determine the thrust direction and the maneuver time that maximize the terminal mass of satellites, that is, minimize the following objective function:

$$J = -\sum_{j=1}^{N_s} m_j(t_{j,f}) \tag{16}$$

This optimization problem is subject to constraints on relative motion dynamics, the given initial and final condition constraints, and the path and linking constraints. The details of these constraints are given in the following subsections.

A. Initial Condition Constraints

The initial conditions for the trajectory optimization are the initial relative state and the initial mass of each deputy satellite. The initial conditions are given as follows:

$$x_j(t_0) = x_{j,0}, \qquad y_j(t_0) = y_{j,0}, \qquad z_j(t_0) = z_{j,0}$$
$$\dot{x}_j(t_0) = \dot{x}_{j,0}, \qquad \dot{y}_j(t_0) = \dot{y}_{j,0}, \qquad \dot{z}_j(t_0) = \dot{z}_{j,0} \tag{17}$$

$$m_j(t_0) = m_{j,0} \tag{18}$$

B. Final Condition Constraints

A few published works deal with the final conditions of trajectory optimization for satellite formation, but most of them set the final states of satellites as a priori fixed points. Richards et al. [8] defined many subsets of final states and performed the assessment for all subsets within the trajectory optimization process. Subsequently, the subset requiring the lowest overall fuel cost is selected. Huntington et al. [13] derived the final configuration constraints for tetrahedral formation. Two methods to deal with the final condition constraints are studied and compared in this paper. In the first method, the final relative states are treated as variables in the optimization and are subjected to final geometry configuration constraints and the energy-matching condition to obtain the bounded desired final formation. In the second method, the final relative states are given as fixed points determined a priori by using an analytic [26] or a numerical [21,27] formation design method. The analytic formation design method proposed by Sabol et al. [26] is used in this paper. It can be seen from the simulation results presented later in the paper that the first method can result in lower fuel consumption than the second method.

The energy-matching condition considering nonlinearity and orbit eccentricity for bounded relative satellite motion is derived by Gurfil [28]. This energy-matching constraint imposed at the end of maneuvers for each satellite, shown in Eq. (19), is included in the optimization to obtain a bounded final formation. (Incidentally, the energy-matching condition considering the J_2 effect based on our recently obtained exact nonlinear relative satellite dynamics model is presently under development.)

$$\left|\tfrac{1}{2}\{(\dot{x}_{j,f} - \omega_{z,f}y_{j,f} + \dot{r}_f)^2 + [\dot{y}_{j,f} + \omega_{z,f}(x_{j,f} + r_f)]^2 + \dot{z}_{j,f}^2\} - \mu/\sqrt{(r_f + x_{j,f})^2 + y_{j,f}^2 + z_{j,f}^2} + \mu/2a\right| \le \varepsilon_1 \tag{19}$$

where ε_1 is a very small number that ensures that the optimization is feasible.

It is impossible to derive final geometry configurations for the general formation. Circular formation and projected circular formation are the two most-studied satellite formations [26]. The final geometry configuration constraints are derived for circular formation

with three deputy satellites evenly spaced in a circle. These constraints can be easily extended to projected circular formation.

For circular formation, one of the geometry constraints is

$$\left|\sqrt{x_j^2+y_j^2+z_j^2}-R\right|\le \varepsilon_2 \tag{20}$$

where ε_2 is a very small number that ensures that the optimization is feasible, because an exact circular formation does not exist when the chief satellite is in an elliptic orbit. Note that this constraint imposed only on the final state is not sufficient to establish a circular formation. This constraint should also be imposed on several relative positions during one orbital period after the maneuver.

There are two planes on which the circular formation is possible. Both planes intersect the cross-track/along-track plane along the along-track axis, but one is inclined at a positive angle to that plane and the other is inclined at a negative angle. So another geometry constraint, as shown in Eq. (21), should be included to obtain the final formation in a specified plane:

$$\begin{cases} x_{j,f}z_{j,f}>0 \text{ for plane inclined at a positive angle} \\ \text{or} \quad x_{j,f}z_{j,f}<0 \text{ for plane inclined at a negative angle} \end{cases} \tag{21}$$

For the formation with three deputy satellites evenly spaced in the circle, the following constraints should also be included to ensure that the three satellites are evenly spaced in the circle:

$$d_{12}(t_f)=d_{13}(t_f)=d_{23}(t_f) \tag{22}$$

where $d_{p,q}$ denotes the distance between satellite p and satellites q.

C. Path Constraints

First, a collision between the satellites should be avoided during the maneuver, and so the following inequality constraints should be imposed on the relative positions:

$$d_{p,q}(t)\ge d_{\text{safe}}(t), \quad \forall\ p,q\in[1,2,\cdots,N_s],\ p\ne q, \quad \forall\ t\in[t_0,t_f] \tag{23}$$

Second, the mass of each satellite cannot fall below the dry mass. Defining the dry mass of the each satellite as $m_{j,\text{dry}}$, the following inequality constraints should be imposed on the mass of each satellite during the whole trajectory:

$$m_j(t)\ge m_{j,\text{dry}}, \quad \forall\ t\in[t_0,t_f] \tag{24}$$

Last, it is necessary to constrain the thrust direction vector to a constant unit length during the burn phase of the trajectory, as follows:

$$u_{j,x}^2(t)+u_{j,y}^2(t)+u_{j,z}^2(t)=1, \quad \forall\ t\in[t_0,t_f] \tag{25}$$

D. Linking Constraints

To reduce fuel consumption during the maneuver, the thruster can fire several times such that the trajectory can be divided into several phases, including coast and burn phases. During the coast phase the thruster is turned off, whereas during the burn phase the thrust is constant at its maximum value but the thrust direction is steerable. Thus, it is necessary to enforce linkage conditions at every phase boundary to ensure that the trajectory and mass of each satellite are continuous at the interface. These linkage conditions are enforced on the relative position, relative velocity, mass, and time and are given as follows:

$$\begin{gathered} x_j(t_f^v)=x_j(t_0^{v+1}), \qquad y_j(t_f^v)=y_j(t_0^{v+1}), \qquad z_j(t_f^v)=z_j(t_0^{v+1}) \\ \dot{x}_j(t_f^v)=\dot{x}_j(t_0^{v+1}), \qquad \dot{y}_j(t_f^v)=\dot{y}_j(t_0^{v+1}), \qquad \dot{z}_j(t_f^v)=\dot{z}_j(t_0^{v+1}) \\ m_j(t_f^v)=m_j(t_0^{v+1}); \qquad t_{j,f}^v=t_{j,0}^{v+1} \end{gathered} \tag{26}$$

The initial time and the terminal time of each phase are free, but the initial time of the first phase is fixed. To ensure that the time is increasing during the trajectory, the following inequality constraints are imposed on the time during each phase of the trajectory:

$$t_{j,f}^v>t_{j,0}^v \tag{27}$$

IV. Legendre Pseudospectral Method

As noted earlier, the LPM has been widely used over the last few years to solve a variety of optimal control problems. A detailed description of the LPM for solving optimal control problems is provided in [16]. A brief review of this numerical method is given here.

The aforementioned single-phase trajectory optimization problem can be written in the following general form. Determine the control direction, the maneuver time, and the corresponding state trajectory that minimize the following cost function:

$$J(\mathbf{x},\mathbf{u},t_f)=M[\mathbf{x}(t_f),t_f] \tag{28}$$

with $\mathbf{x}\in R^{N_x}$ and $\mathbf{u}\in R^{N_u}$ subject to the following dynamic constraint:

$$\dot{\mathbf{x}}(t)=f[\mathbf{x}(t),\mathbf{u}(t)], \qquad t\in[t_0,t_f] \tag{29}$$

and boundary conditions

$$\psi_{0l}\le\psi_0[\mathbf{x}(t_0),t_0]\le\psi_{0u} \tag{30}$$

$$\psi_{fl}\le\psi_f[\mathbf{x}(t_f),t_f]\le\psi_{fu} \tag{31}$$

where $\psi_0\in R^p$ with $p\le n$, $\psi_f\in R^q$ with $q\le n$, and mixed state-control path constraint

$$h_l\le h[\mathbf{x}(t),\mathbf{u}(t),t]\le h_u \tag{32}$$

It is assumed that these functions are continuously differentiable with respect to their arguments.

The trajectory optimization problem can be discretized into nonlinear programming by the LPM. In the LPM, the LGL points are used. These points, τ_l, $l=0,\ldots,N$, which are distributed on the interval $[-1,1]$, are defined as

$$\tau_0=-1, \qquad \tau_N=1 \tag{33}$$

and, for $1\le l\le N-1$, τ_l are the zeros of $\dot{L}_N$, the derivative of the Legendre polynomial L_N. The discretization process begins by approximating the continuous state and control variables by Nth polynomials of the form.

$$\mathbf{x}(\tau)\approx\mathbf{x}^N(\tau)=\sum_{l=0}^{N}\mathbf{x}(\tau_l)\phi_l(\tau) \tag{34}$$

$$\mathbf{u}(\tau)\approx\mathbf{u}^N(\tau)=\sum_{l=0}^{N}\mathbf{u}(\tau_l)\phi_l(\tau) \tag{35}$$

where, for $l=0,1,\ldots,N$,

$$\phi_l(\tau)=\frac{1}{N(N+1)L_N(\tau_l)}\frac{(\tau^2-1)\dot{L}_N(\tau)}{\tau-\tau_l} \tag{36}$$

are the Lagrange interpolating polynomials of order N.

The dynamic equations are discretized by imposing the condition that the derivatives of the state approximations satisfy the differential equations exactly at the node points. Thus, the derivative of $\mathbf{x}^N(\tau)$ in terms of $\mathbf{x}(\tau)$ at the collocation point τ_k can be obtained by differentiating Eq. (34) and evaluating the result at τ_k. The result is a matrix multiplication given by

$$\dot{\mathbf{x}}(\tau_k)\approx\dot{\mathbf{x}}^N(\tau_k)=\sum_{l=0}^{N}\mathbf{x}(\tau_l)\dot{\phi}_l(\tau_k)=\sum_{l=0}^{N}D_{kl}\mathbf{x}(\tau_l) \tag{37}$$

where $D_{kl} = \dot{\phi}_l(\tau_k)$ are the entries of the $(N+1) \times (N+1)$ differentiation matrix $\mathbf{D}$:

$$\mathbf{D} := [D_{kl}] := \begin{cases} \frac{L_N(\tau_k)}{L_N(\tau_l)} \frac{1}{\tau_k - \tau_l} & k \neq l \\ -\frac{N(N+1)}{4} & k = l = 0 \\ \frac{N(N+1)}{4} & k = l = N \\ 0 & \text{otherwise} \end{cases} \tag{38}$$

The mixed state-control path constraints and the boundary conditions can also be discretized by evaluating these inequalities at the LGL nodes. Thus, the single-phase trajectory optimization problem can now be discretized as follows.

Find the $(N+1)(N_x + N_u) + 1$ vector $\boldsymbol{X}_{\text{opt}}$:

$$\mathbf{X}_{\text{opt}} = [\mathbf{x}(\tau_0), \mathbf{x}(\tau_1), \ldots, \mathbf{x}(\tau_N); \mathbf{u}(\tau_0), \mathbf{u}(\tau_1), \ldots, \mathbf{u}(\tau_N); t_f] \tag{39}$$

which minimizes

$$J(\mathbf{X}_{\text{opt}}) = M(\mathbf{x}(\tau_N), t_f) \tag{40}$$

subject to

$$\sum_{l=0}^{N} D_{kl}\mathbf{x}(\tau_l) - \frac{t_f - t_0}{2} f(\mathbf{x}(\tau_k), \mathbf{u}(\tau_k), \tau_k) = 0 \tag{41}$$

$$\psi_{0l} \leq \psi_0(\mathbf{x}(\tau_0), \tau_0) \leq \psi_{0u} \tag{42}$$

$$\psi_{fl} \leq \psi_f(\mathbf{x}(\tau_N), \tau_N) \leq \psi_{fu} \tag{43}$$

$$h_l \leq h_k(\mathbf{x}(\tau_k), \mathbf{u}(\tau_k)) \leq h_u \qquad k = 0, \ldots, N \tag{44}$$

The LPM can be extended to problems with multiple phases in a straightforward manner [22]. The pseudospectral implementation of trajectory optimization with multiple phases is treated by defining each phase separately and then linking these phases with a set of phase boundary conditions.

V. Computational Considerations

This section discusses issues related to the implementation and solution of the optimization problem presented in the preceding sections. The methods presented here do not change the basic constraints already described, but assist greatly in obtaining solutions within a practical and reasonable computational time interval.

A. Scaling

Scaling a nonlinear programming problem is very important to obtain a robust and rapid convergence to the final solution. Betts [29] commented that "Scaling affects everything! Poor scaling can make a good algorithm bad. Scaling changes the convergence rate, termination tests, and numerical conditioning." One way to construct a well-scaled problem is to normalize the independent variables to have the same range [29]. For example, $0 \leq \tilde{x}_k \leq 1$, where $\tilde{x}_k$ denotes the scaled variables. Thus, the following normalizations are used in this work:

$$\tilde{x} = x/d_{\max}, \qquad \tilde{y} = y/d_{\max}, \qquad \tilde{z} = z/d_{\max} \tag{45}$$

$$\tilde{m} = m/m_0, \qquad \tilde{t} = t/T_c \tag{46}$$

The magnitude of the maximum relative velocities during a maneuver is on the order of 1, and so it is not necessary to normalize the relative velocities.

B. Initial Guess

The LPM has a larger radius of convergence than other numerical methods, and it may not require a good initial guess for convergence. However, an educated initial guess does improve the convergence rate and robustness.

In this paper, an initial guess is generated by integrating the relative dynamics numerically using an arbitrary control direction. The generated states and control direction thus satisfy the initial conditions and the differential dynamic constraints, but do not satisfy the terminal constraints and are generally nonoptimal. Using this initial guess, TOMLAB/SNOPT is able to solve the resulting NLP problems within several minutes. A better initial guess could be the optimized trajectory solution obtained for a relative dynamics model such as Hill's equations. The trajectory generated by our present algorithm without considering a collision avoidance constraint would also provide a good initial guess for the trajectory optimization problem with a collision avoidance constraint.

C. Implementation

The optimization was carried out with the TOMLAB$^{\text{TM}}$ version of the NLP solver SNOPT using default optimality and feasibility tolerances. TOMLAB/SNOPT is a software package for solving large-scale optimization problems (linear and nonlinear programs) [24]. It is especially effective for nonlinear problems for which the functions and gradients are expensive to evaluate. Thus, TOMLAB/SNOPT is well suited to solve the proposed trajectory optimization problem after it is transcribed into a large-scale nonlinear programming problem.

VI. Numerical Results

In this section, examples are presented for a wide class of satellite formation reconfiguration problems. First, formation reconfigura-

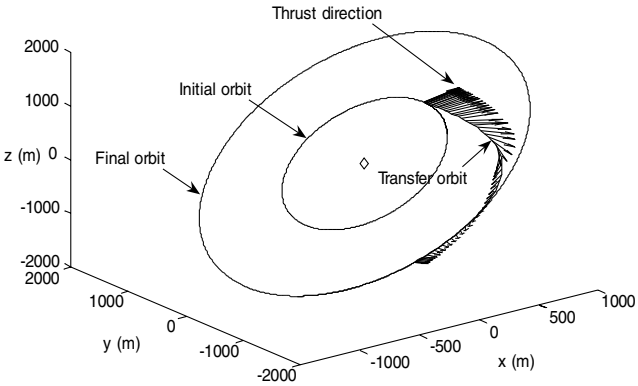

Fig. 2 Trajectories of formation reconfiguration with a free relative final state.

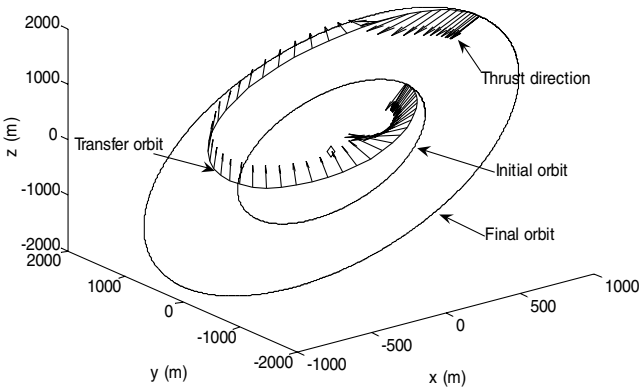

Fig. 3 Trajectories of formation reconfiguration with given final relative states.

Table 1 Fuel consumption and maneuver time for the single-phase maneuver

	Fuel consumption		Maneuver time, s
	Δm, kg	ΔV, m/s	
Free final state	0.01131	2.217	2221
Fixed final state	0.02190	4.292	4283

tions involving two satellites (one chief satellite and one deputy satellite) are studied. As mentioned earlier, to conserve fuel during the maneuver, the thruster can be fired several times during the trajectory according to a certain phase sequence. Trajectory optimizations with the following different phase sequences are studied and compared: 1) one phase: burn, 2) two phases: coast-burn, 3) three phases: burn-coast-burn, and 4) four phases: coast-burn-coast-burn.

Second, formation reconfigurations involving multiple satellites, such as four satellites, are studied. Finally, the collision avoidance capability of the proposed method is also demonstrated.

The chief satellite orbit is characterized by the following orbit elements:

$$a = 7100 \text{ km}, \quad e = 0.001, \quad i = 45 \text{ deg}, \quad \omega = 30 \text{ deg}$$
$$\Omega = 45 \text{ deg}, \quad f = 0 \text{ deg} \tag{47}$$

All the deputy satellites have been considered with the same following parameters:

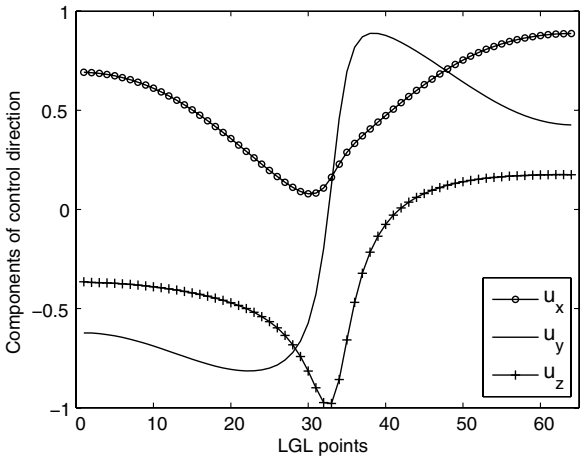

Fig. 4 Control direction.

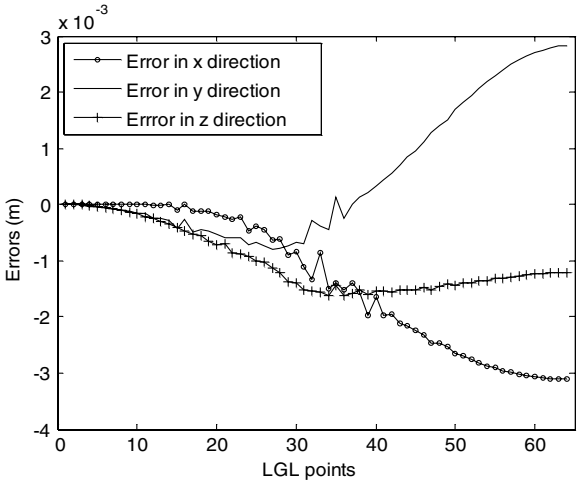

Fig. 5 Error history with dynamics considering the J_2 perturbation.

$$m_0 = 50 \text{ kg}, \quad T = 50 \text{ mN}, \quad I_{sp} = 1000 \text{ s} \tag{48}$$

This control force can be realized with an actual electric propulsion system [6].

A. Two Satellites, One Burn Phase

In this example, the deputy satellite in a circular formation with a 1000 m radius is maneuvered to another circular formation with radius of 2000 m. During this maneuver with one burn phase, the thrust is constant at its maximum value. The number of LGL points is chosen as 64. More accurate results can be obtained in this NLP problem with more LGL points at the expense of computational cost. The optimization can be completed within 30 s even without using analytic first-order derivatives for both the Jacobian matrices of the constraint conditions and the gradient of the objective function. The initial relative state of the deputy satellite with respect to the chief satellite is given as follows:

$$x_0 = 500 \text{ m}, \quad \dot{x}_0 = 0 \text{ m/s}, \quad y_0 = 0 \text{ m}, \quad \dot{y}_0 = 1 \text{ m/s}$$
$$z_0 = 866.0254 \text{ m}, \quad \dot{z}_0 = 0 \text{ m/s} \tag{49}$$

As noted earlier, two different methods of handling the final condition constraints are considered. In the first method, the final relative state is treated as a variable in the optimization problem and subjected to final geometry configuration constraints and an energy-matching condition to obtain the bounded desired final formation. In the second method, the final relative state is determined by an analytic formation design method [26]. The computed final relative state for the second method is given as follows:

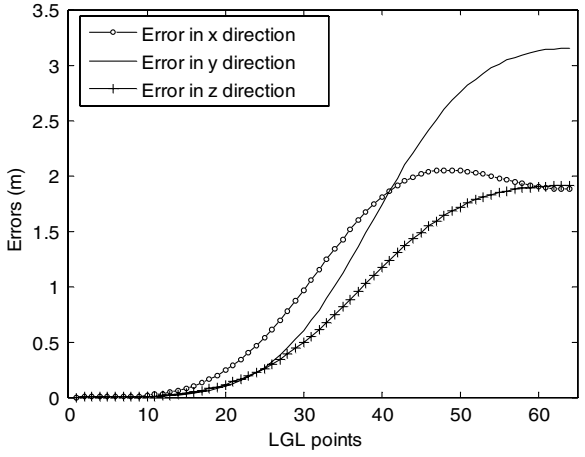

Fig. 6 Error history with dynamics not considering the J_2 perturbation.

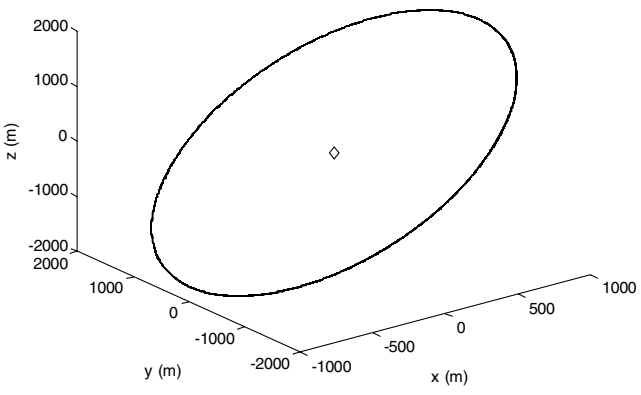

Fig. 7 Trajectories of final formation propagated for one day.

Table 2 Computation times and maximum position errors for the LPM and GPM

	CPU times, s		Max. position error, m	
N	LPM	GPM	LPM	GPM
15	3.06	4.08	2.802×10^{-1}	3.420×10^{-1}
30	10.21	8.06	1.65×10^{-2}	1.54×10^{-2}
45	17.20	16.06	2.7×10^{-3}	3.0×10^{-3}

Table 3 Fuel consumption and maneuver time for the two-phase maneuver

	Fuel consumption		Maneuver time, s	
Cases	Δm, kg	ΔV, m/s	Coast	Burn
Free final state	0.01046	2.050	5255	2050
Fixed final state	0.01069	2.095	4149	2095

$$x_f = 1000 \text{ m}, \quad \dot{x}_f = 0 \text{ m/s}, \quad y_f = 0 \text{ m}, \quad \dot{y}_f = 2 \text{ m/s}$$
$$z_f = 1732.1 \text{ m}, \quad \dot{z}_0 = 0 \text{ m/s} \tag{50}$$

The fuel-optimal trajectories generated for the two cases are shown in Figs. 2 and 3, respectively. Maneuver time and fuel consumption are shown in Table 1. For ease of interpretation, ΔV is calculated approximately by assuming a constant mass of the satellite during the formation maneuver. As observed from the results, the first method results in a fuel savings of 48.35% as compared with the second method. Thus, it can be concluded that, for formation maneuver with a single burn phase, the first method, with substantially lower fuel consumption, is much better than the second method. The components of the control direction for the first method are shown in Fig. 4.

An open-loop guidance demonstration is performed using the control direction generated by the LPM. The LPM gives a state estimation and control only at the LGL points. Cubic spline interpolation is used to estimate the controls between the LGL points. In the simulation, the optimized control force is executed on the deputy satellite in an open-loop way, with no in-flight corrections, and the actual relative trajectory is generated by integrating the absolute equation of motion including the J_2 effect for each satellite using the MATLAB® command ODE45. The errors between the actual trajectory and the optimized trajectory are plotted in Fig. 5. For comparison, another trajectory is generated by the LPM using nonlinear relative dynamics without the J_2 effect. The errors between the actual trajectory and this optimized trajectory are shown in Fig. 6. As can be observed from the results, the errors with relative dynamics considering the J_2 effect are much smaller than those without considering the J_2 effect. It can be concluded that a nonlinear relative satellite dynamics model considering the J_2 effect is necessary to obtain a high-precision trajectory for satellite formation maneuvers.

To validate the effectiveness of the energy-matching condition in obtaining a bounded final formation, the generated final formation is propagated in the dynamics environment without considering the J_2 effect for 24 h. The propagated formation is plotted in Fig. 7. As can be seen from the results, the drift of the formation is very small, and a bounded formation is obtained. As noted earlier, the exact energy-matching condition considering the J_2 effect is presently under development.

Another kind of pseudospectral method developed for solving trajectory optimization problem is the Gauss pseudospectral method [30], which is similar to the LPM. To further validate the efficiency of the pseudospectral method in designing fuel-optimal maneuvers for the satellite formation reconfiguration problem, the GPM is also

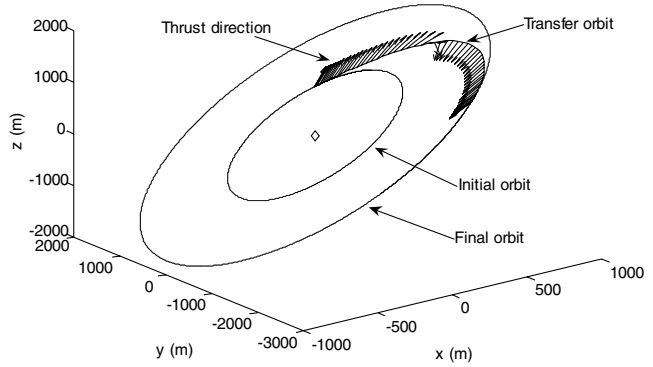

Fig. 8 Trajectories of formation reconfiguration with a free relative final state.

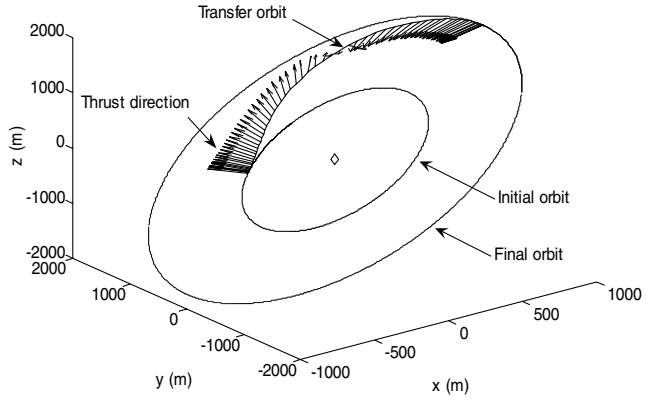

Fig. 9 Trajectories of formation reconfiguration with a given relative final state.

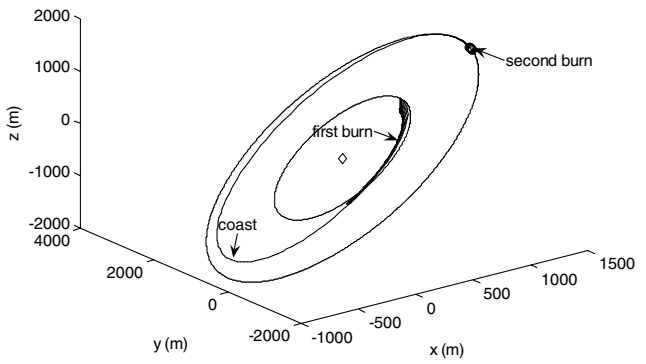

Fig. 10 Trajectories of formation reconfiguration with a free relative final state.

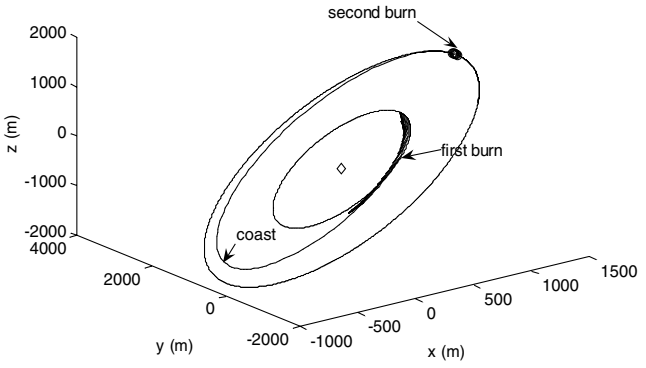

Fig. 11 Trajectories of formation reconfiguration with a given relative final state.

Table 4 Fuel consumption and maneuver time for the three-phase maneuver

	Fuel consumption		Maneuver time, s			
Cases	Δm, kg	ΔV, m/s	1st burn	Coast	2nd burn	Total
Free final state	0.006671	1.308	1243	4692	65	6000
Fixed final state	0.006698	1.313	1248	4429	64	5741

used to solve the aforementioned formation reconfiguration problem with an equivalent initial guess as for the LPM. Relative position error histories for the LPM and GPM are generated using the open-loop guidance method, as in the example given. Maximum relative position errors and computational times are shown in Table 2. It can be seen from Table 2 that the LPM and GPM are comparable in computational efficiency and trajectory accuracy. Note that it is shown in [31] that the GPM can produce significantly more accurate costate estimations than the LPM without incurring an additional computational burden.

B. Two Satellites, Two Phases: Coast-Burn

In this example, the formation maneuver mission, the initial and final conditions are the same as those in the previous example. The only difference is the phase sequence. Before the burn phase, one coast phase is added to the trajectory so that the satellite can choose the right time to leave the original formation so as to save fuel. The number of LGL points for each phase is 64. Fuel-optimal trajectories generated by using the two different methods dealing with final condition constraints are plotted in Figs. 8 and 9, respectively. Coast time, burn time, and fuel consumption are shown in Table 3. As seen from the simulation results, the maneuver with two phases can save about half the fuel required by that with a single burn phase.

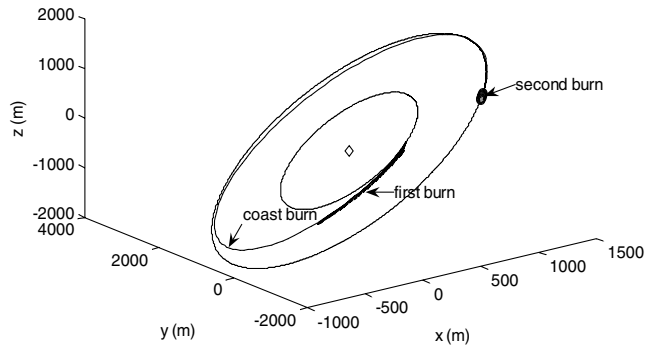

Fig. 12 Trajectories of formation reconfiguration with a free relative final state.

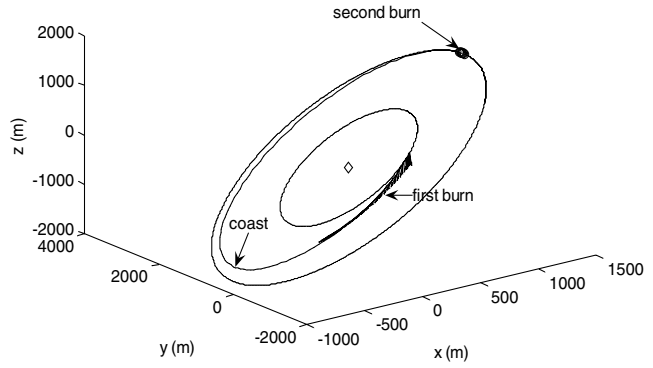

Fig. 13 Trajectories of formation reconfiguration with a given relative final state.

Table 5 Fuel consumption and maneuver time for the four-phase maneuver

	Fuel consumption		Maneuver time, s			
Cases	Δm, kg	ΔV, m/s	1st coast	1st burn	2nd coast	2nd burn
Free final state	0.005181	1.016	1146	946	4198	73
Fixed final state	0.005357	1.050	1053	988	4146	65

C. Two Satellites, Three Phases: Burn-Coast-Burn

In this example, the trajectory is divided into three phases: burn, coast, and burn. Fuel-optimal trajectories generated by using the two different methods dealing with final condition constraints are shown in Figs. 10 and 11, respectively. Maneuver time and fuel consumption are shown in Table 4. As observed from the results, the first method uses 0.4% less fuel than the second method, and the maneuver with three phases requires less fuel than the maneuver with two phases.

D. Two Satellites, Four Phases: Coast-Burn-Coast-Burn

In this example, the trajectory is divided into four phases: coast, burn, coast, and burn. Fuel-optimal trajectories generated by using the two different methods dealing with final condition constraints are plotted in Figs. 12 and 13, respectively. Coast times, burn times, and the fuel consumption in each case are shown in Table 5. It is observed from the results that the first method can save 3.4% more fuel as compared with the second method, and a maneuver with four phases requires less fuel than a maneuver with three phases.

E. Formation Reconfiguration Involving Four Satellites

This example validates the applicability of the proposed trajectory optimization method for multisatellite formation. Formation reconfiguration is studied for a formation with four satellites (one chief satellite and three deputy satellites). The three deputy satellites are maneuvered from a circular formation with a radius of 1000 m to another circular formation with a radius of 2000 m, and the three deputy satellites are evenly spaced in the final circular formation. The initial relative state of each deputy satellite is as follows:

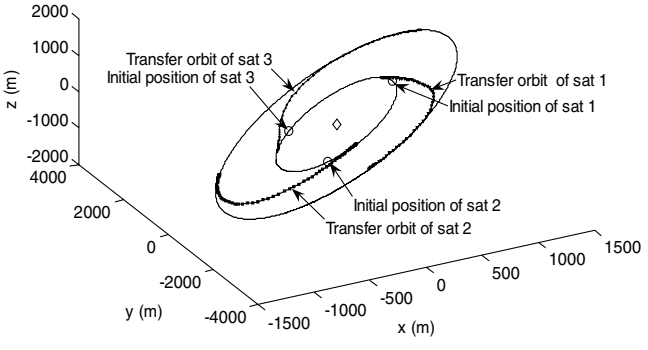

Fig. 14 Trajectories of formation reconfiguration of four satellites.

Table 6 Fuel consumption and maneuver time for the four-satellite formation

Deputy satellite 1				Deputy satellite 2				Deputy satellite 3			
Fuel		Time, s		Fuel		Time, s		Fuel		Time, s	
Δm, kg	ΔV, m/s	Coast	Burn	Δm, kg	ΔV, m/s	Coast	Burn	Δm, kg	ΔV, m/s	Coast	Burn
0.01063	2.083	5918	2081	0.01087	2.131	5821	2131	0.01077	2.111	5804	2110

$$
\begin{aligned}
&x_{1,0}=500, \quad \dot{x}_{1,0}=0, \quad y_{1,0}=0, \quad \dot{y}_{1,0}=1\\
&z_{1,0}=866, \quad \dot{z}_{1,0}=0 \quad x_{2,0}=-250, \quad \dot{x}_{2,0}=0.433\\
&y_{2,0}=866, \quad \dot{y}_{2,0}=0.5, \quad z_{2,0}=433, \quad \dot{z}_{2,0}=0.75\\
&x_{3,0}=-250, \quad \dot{x}_{3,0}=0.433, \quad y_{3,0}=-866, \quad \dot{y}_{3,0}=0.5\\
&z_{3,0}=433, \quad \dot{z}_{3,0}=-0.75
\end{aligned} \tag{51}
$$

where the unit of relative positions is in meters and that of the relative velocities is in meters per second.

As can be concluded from the earlier examples, for a maneuver with more than one phase, the optimization with a free final state does not result in significant fuel saving as compared with that with fixed final state. Thus, we propose to determine and fix the final state for a maneuver with multiple phases. In this example, the final relative states satisfying the desired final formation are given in Eq. (52) by applying the analytic formation design method [26], and the trajectory is divided into two phases (coast-burn).

$$
\begin{aligned}
&x_{1,f}=-110.8, \quad \dot{x}_{1,f}=-0.9942, \quad y_{1,f}=-1988.7\\
&\dot{y}_{1,f}=0.2216, \quad z_{1,f}=-191.4, \quad \dot{z}_{1,f}=-1.7195\\
&x_{2,f}=914.4, \quad \dot{x}_{2,f}=0.4051, \quad y_{2,f}=800.6\\
&\dot{y}_{2,f}=-1.8289, \quad z_{2,f}=1587.1, \quad \dot{z}_{2,f}=0.6940\\
&x_{3,f}=-806.9, \quad \dot{x}_{3,f}=0.5918, \quad y_{3,f}=1183.3\\
&\dot{y}_{3,f}=1.6138, \quad z_{3,f}=-1394.9, \quad \dot{z}_{3,f}=1.0231
\end{aligned} \tag{52}
$$

where the unit of relative positions is in meters and that of the relative velocities is in meters per second.

Fuel-optimal trajectories generated for the three deputy satellites are shown in Fig. 14. The corresponding maneuver times and fuel consumptions are shown in Table 6.

F. Collision Avoidance Validation

The final example demonstrates the effectiveness of the proposed method in meeting the collision avoidance requirement. The three

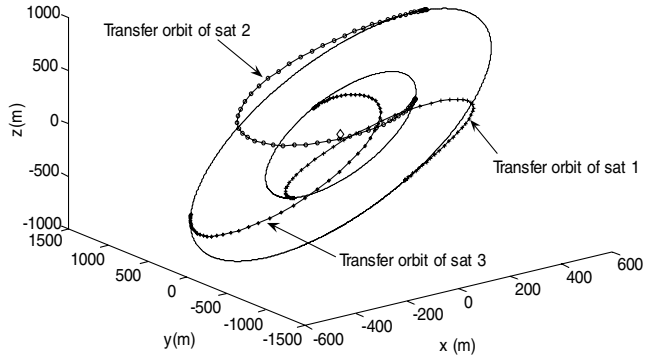

Fig. 15 Trajectories of formation maneuver without collision avoidance constraints.

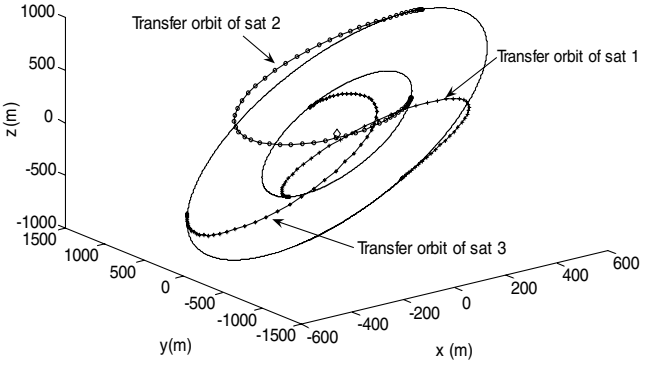

Fig. 17 Trajectories of formation with collision avoidance constraints.

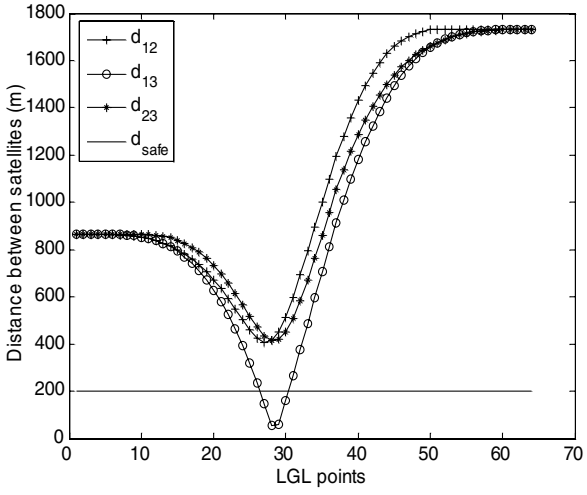

Fig. 16 Satellite relative distances during maneuver without collision avoidance constraints.

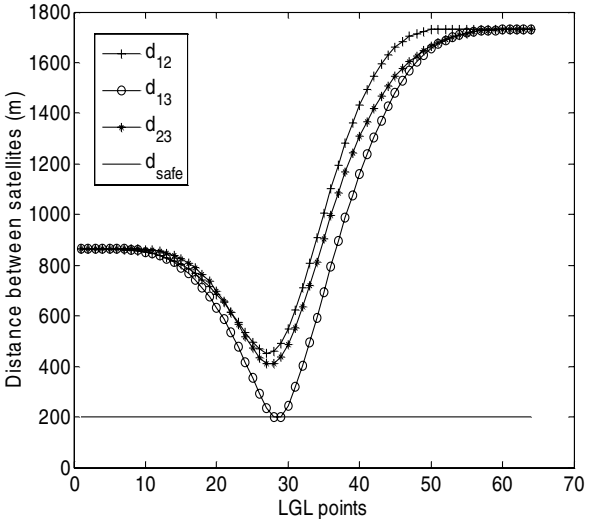

Fig. 18 Satellite relative distances during maneuver with collision avoidance constraints.

Table 7 Fuel consumption of each satellite during maneuvers

	Fuel consumption, satellite 1		Fuel consumption, satellite 2		Fuel consumption, satellite 3	
	Δm, kg	ΔV, m/s	Δm, kg	ΔV, m/s	Δm, kg	ΔV, m/s
First maneuver	0.0255	4.998	0.0256	5.018	0.0255	4.998
Second maneuver	0.0258	5.057	0.0278	5.449	0.0267	5.233

deputy satellites are maneuvered from a circular formation with a radius of 500 m to another circular formation with a radius of 1000 m using only one burn phase. The initial and final positions as well as the velocities are chosen a priori.

The optimized trajectories of each satellite obtained without considering collision avoidance are shown in Fig. 15, and the distances between the deputy satellites during the maneuver are plotted in Fig. 16. As observed from the simulation results, the smallest distance between satellites 1 and 3 is only 43 m. This separation is hazardous, and so a collision avoidance constraint should be included in the optimization. In the ensuring optimization problem, the safe distance is assumed to be $d_{\text{safe}} = 200$ m. The optimized trajectories obtained by incorporating the collision avoidance requirement are shown in Fig. 17, and the corresponding distances between the deputy satellites during the maneuver are shown in Fig. 18. As seen from the results, the distances between the satellites are always greater than the required safe distance. It can be concluded that the proposed method can perform safe formation maneuvers. As observed from Table 7, the fuel consumption for the two cases are almost the same, but the method that incorporates the collision avoidance constraints can guarantee collision avoidance during the maneuver.

VII. Conclusions

An efficient method of designing fuel-optimal trajectories for satellite formation deployment/reconfiguration with a collision avoidance requirement is proposed in this paper. High-precision maneuver trajectories are obtained by using our recently developed exact relative satellite motion model, which incorporates eccentricity, nonlinearity, and Earth oblateness effects. Bounded desired final satellite formations are ensured by including an energy-matching condition and final geometry configuration constraints in the optimization formulation. Using the LPM, the trajectory optimization problem is reduced into a nonlinear programming problem, which is solved numerically by TOMLAB/SNOPT. Extensive simulation results demonstrate the effectiveness of the proposed methodology for several realistic satellite formation deployment/reconfiguration problems involving nonlinear dynamics under the J_2 influence.

The proposed approach yields an optimal open-loop solution for satellite formation maneuvers that have potential applications in satellite formation mission design and analysis. Further investigations are required to render the proposed approach amenable to onboard real-time guidance and control applications. In particular, it has to be integrated with a closed-loop control design to ensure optimal trajectory path following despite system uncertainties and external perturbations. Our current research effort is focused on adapting the approach developed in this paper to solve this closed-loop design problem.

Acknowledgment

This paper was funded in part by project agreement no. POD0513235 of the Singapore Defense of Science and Technology Agency.

References

[1] Scharf, D. P., Hadaegh, F. Y., and Ploen, S. R., "A Survey of Spacecraft Formation Flying Guidance and Control (Part 1): Guidance," *Proceedings of the 2003 American Control Conference*, Vol. 2, American Automatic Control Council, Dayton, OH, June 2003, pp. 1733–1739.

[2] Schaub, H., and Alfriend, K. T., "Impulsive Feedback Control to Establish Specific Mean Orbit Elements of Spacecraft Formations," *Journal of Guidance, Control, and Dynamics*, Vol. 24, No. 4, 2001, pp. 739–745. doi:10.2514/2.4774

[3] Vaddi, S. S., Alfriend, K. T., Vadali, S. R., and Sengupta, P., "Formation Establishment and Reconfiguration Using Impulsive Control," *Journal of Guidance, Control, and Dynamics*, Vol. 28, No. 2, 2005, pp. 262–268. doi:10.2514/1.6687

[4] Lovell, T. A., and Tragesser, S. G., "Analysis of the Reconfiguration and Maintenance of Close Spacecraft Formations," American Astronautical Society Paper 03-139, Feb. 2003.

[5] Pillet, N., Bousquet, P., Chesta, E., Cledassou, R., Delpech, M., and Hinglais, E., "Propulsion Options for Preliminary Formation Flying Missions Studies at CNES," AIAA Paper 2006-5221, July 2006.

[6] Pencil, E. J., Kamhawi, H. K., and Arrington, L. A., "Overview of NASA's Pulsed Plasma Thruster Development Program," AIAA Paper 2004-3455, July 2004.

[7] Tillerson, M., Inalhan, G., and How, J. P., "Coordination and Control of Distributed Spacecraft Systems Using Convex Optimization Techniques," *International Journal of Robust and Nonlinear Control*, Vol. 12, No. 2–3, 2002, pp. 207–242. doi:10.1002/rnc.683

[8] Richards, A., Schouwenaars, T., How, J., and Feron, E., "Spacecraft Trajectory Planning with Avoidance Constraints Using Mixed-Integer Linear Programming," *Journal of Guidance, Control, and Dynamics*, Vol. 25, No. 4, 2002, pp. 755–764. doi:10.2514/2.4943

[9] Açıkmeşe, B., Scharf, D. P., Murray, E. A., and Hadaegh, F. Y., "A Convex Guidance Algorithm for Formation Reconfiguration," AIAA Paper 2006-6070, Aug. 2006.

[10] Campbell, M. E., "Planning Algorithm for Large Satellite Clusters," *Journal of Guidance, Control, and Dynamics*, Vol. 26, No. 5, 2003, pp. 770–780. doi:10.2514/2.5111

[11] Zanon, D. J., and Campbell, M. E., "Optimal Planner for Spacecraft Formations in Elliptical Orbits," *Journal of Guidance, Control, and Dynamics*, Vol. 29, No. 1, 2006, pp. 161–171. doi:10.2514/1.7236

[12] Milam, M. B., Petit, N., and Murray, R. M., "Constrained Trajectory Generation for Micro-Satellite Formation Flying," AIAA Paper 2001-4030, Aug. 2001.

[13] Huntington, G. T., Benson, D. A., and Rao, A. V., "Design of Optimal Tetrahedral Spacecraft Formations," *Journal of the Astronautical Sciences*, Vol. 55, No. 2, 2007, pp. 141–169.

[14] Huntington, G. T., and Rao, A. V., "Optimal Reconfiguration of Spacecraft Formations Using the Gauss Pseudospectral Method," *Journal of Guidance, Control, and Dynamics*, Vol. 31, No. 3, 2008, pp. 689–698. doi:10.2514/1.31083

[15] Mauro, M., and Franco, B. Z., "Optimization of Low-Thrust Trajectories for Formation Flying with Parallel Multiple Shooting," AIAA Paper 2006-6747, Aug. 2006.

[16] Elnagar, G., Kazemi, M., and Razzaghi, M., "The Pseudospectral Legendre Method for Discretizing Optimal Control Problems," *IEEE Transactions on Automatic Control*, Vol. 40, No. 10, 1995, pp. 1793–1796. doi:10.1109/9.467672

[17] Betts, J. T., "Survey of Numerical Methods for Trajectory Optimization," *Journal of Guidance, Control, and Dynamics*, Vol. 21, No. 2, 1998, pp. 193–207. doi:10.2514/2.4231

[18] Qi, G., Kang, W., and Ross, I. M., "A Pseudospectral Method for the Optimal Control of Constrained Feedback Linearizable System," *IEEE Transactions on Automatic Control*, Vol. 51, No. 7, 2006, pp. 1115–1129. doi:10.1109/TAC.2006.878570

[19] Rao, A. V., and Clarke, K. A., "Performance Optimization of a Maneuvering Re-Entry Vehicle Using a Legendre Pseudospectral Method," AIAA Paper 2002-4885, Aug. 2002.

[20] Stanton, S., and Proulx, R., "Optimal Orbital Transfer Using a Legendre Pseudospectral Method," American Astronautical Society Paper 03-574, Aug. 2003.

[21] Infeld, S. I., Josselyn, S. B., Murray, W., and Ross, I. M., "Design and Control of Libration Point Spacecraft Formations," *Journal of Guidance, Control, and Dynamics*, Vol. 30, No. 4, 2007, pp. 899–909. doi:10.2514/1.18654

[22] Ross, I. M., Souza, C. D., Fahroo, F., and Ross, J. B., "A Fast Approach to Multi-Stage Launch Vehicle Trajectory Optimization," AIAA Paper 2003-5639, Aug. 2003.

[23] Hui, Y., Ross, I. M., and Alfriend, K. T., "Pseudospectral Feedback Control for Three-Axis Magnetic Attitude Stabilization in Elliptic Orbits," *Journal of Guidance, Control, and Dynamics*, Vol. 30, No. 4, 2007, pp. 1107–1115. doi:10.2514/1.26591

[24] Holmström, K., Göran, A. O., and Edvall, M. M., "Users Guide for TOMLAB /SNOPT," Mälardalen University, Dept. of Mathematics and Physics, Västerås, Sweden, Dec. 2006, p. 171.

[25] Xu, G. Y., and Wang, D. W., "Nonlinear Dynamic Equations of Satellite Relative Motion Around an Oblate Earth," *Journal of Guidance, Control, and Dynamics*, Vol. 31, No. 5, 2008, pp. 1521–1524. doi:10.2514/1.33616

[26] Sabol, C., Burns, R., and McLaughlin, C. A., "Satellite Formation Flying Design and Evolution," *Journal of Spacecraft and Rockets*, Vol. 38, No. 2, 2001, pp. 270–278. doi:10.2514/2.3681

[27] Breger, L., and How, J. P., "Partial J_2 Invariant Satellite Formation," AIAA Paper 2006-6585, Aug. 2006.

[28] Gurfil. P., "Relative Motion Between Elliptic Orbits: Generalized Boundedness Conditions and Optimal Formation keeping," *Journal of Guidance, Control, and Dynamics*, Vol. 28, No. 4, 2005, pp. 761–767. doi:10.2514/1.9439

[29] Betts, J. T., *Practical Methods for Optimal Control Using Nonlinear Programming*, Society for Industrial and Applied Mathematics, Philadelphia, 2001, pp. 121–123.

[30] Benson, D. A., Huntington, G. T., Thorvaldsen, T. P., and Rao, A. V., "Direct Trajectory Optimization and Costate Estimation via an Orthogonal Collocation Method," *Journal of Guidance, Control, and Dynamics*, Vol. 29, No. 6, 2006, pp. 1435–1440. doi:10.2514/1.20478

[31] Huntington, G. T., Benson, D. A., and Rao, A. V., "A Comparison of Accuracy and Computational Efficiency of Three Pseudospectral Methods," AIAA Paper 2007-6405, Aug. 2007.